

Sensitivity of the initiation of an isolated thunderstorm over the Beijing metropolitan region to urbanization, terrain morphology and cold outflows

Huiqi Li,^{a,b} Xiaopeng Cui^{a,b,c*} and Da-Lin Zhang^{d,e}

^aKey Laboratory of Cloud-Precipitation Physics and Severe Storms (LACS), Institute of Atmospheric Physics, Chinese Academy of Sciences, Beijing, China

^bUniversity of Chinese Academy of Sciences, Beijing, China

^cCollaborative Innovation Center on Forecast and Evaluation of Meteorological Disasters, Nanjing University of Information Science & Technology, China

^dState Key Laboratory of Severe Weather, Chinese Academy of Meteorological Sciences, Beijing, China

^eDepartment of Atmospheric and Oceanic Science, University of Maryland, College Park, MD, USA

*Correspondence to: X. Cui, Key Laboratory of Cloud-Precipitation Physics and Severe Storms (LACS), Institute of Atmospheric Physics, Chinese Academy of Sciences, 40 Huayanli, Chaoyang District, Beijing 100029, China. E-mail: xpcui@mail.iap.ac.cn

To gain insight into the processes leading to the convective initiation (CI) of an isolated thunderstorm near the central urban area (CUA) of the Beijing metropolitan region (BMR) on 9 August 2011, a series of numerical sensitivity experiments by removing or modifying the CUA, terrain morphology, and convectively generated cold outflows is performed. Results show that the CUA accounts for the formation of cloud condensation near the top of the mixed layer at the CI site as a result of the growing boundary-layer depth through its urban heat island effects and urban-induced convergence between a warm and moist southerly flow and an easterly flow on the downstream side. The northerly approaching cold outflows from the mesoscale convective system (MCS) facilitate the generation of northerly flows through ‘a northwestward-concave valley’ such that the enhanced low-level convergence with the southerly and easterly flows near the CUA could determine the timing of the outbreak of shallow clouds near the mixed-layer top into an intense thunderstorm. If the concave valley to the northwest of the CUA is eliminated, little northerly flow ahead of the cold outflow boundaries into the CI site would be present. The results obtained herein appear to have significant implications for understanding and forecasting the development of afternoon thunderstorms in the BMR under weak-gradient environments.

Key Words: convective initiation; urbanization; terrain morphology; cold outflows; numerical experiment

Received 30 May 2017; Revised 15 August 2017; Accepted 25 September 2017; Published online in Wiley Online Library 14 November 2017

1. Introduction

Despite extensive research on convective initiation (CI) for improving convective parametrization (Fritsch and Chappell, 1980; Zhang and Fritsch, 1986; Kain, 2004) and nowcasting convective development (Weckwerth and Parsons, 2006) during the past decades, the location, timing and intensity of CI are least well forecast compared to the other aspects of deep moist convection. Johns and Doswell (1992) suggest the following three ingredients for CI: instability or convective available potential energy (CAPE), moisture, and lifting mechanisms. Lifting is important for air parcels to reach the level of free convection in the presence of convective inhibition. The lifting of air parcels for CI is often measured by vertical motion, but it is difficult to accurately obtain due largely to scarce observations, so it has been often inferred by convergence in the planetary boundary layer (PBL). Consideration of the above ingredients suggests that

CI results from complicated multi-scale interactions, including mesoscale and synoptic-scale settings (Johnson and Mapes, 2001), local circulations such as drylines (e.g. Rhea, 1966; Ziegler *et al.*, 1997; Xue and Martin, 2006), lake and sea breezes (e.g. Nicholls *et al.*, 1991; Xu *et al.*, 1996), orography and surface inhomogeneity that dictates local convergence zones (Wulfmeyer *et al.*, 2008), baroclinic zones and convectively generated boundaries as well as gravity waves and bores (Purdom, 1976; Zhang and Fritsch, 1988; Weckwerth and Parsons, 2006; Wilson and Roberts, 2006), in addition to four-dimensional water vapour distribution.

During warm months, some regions may have statistically higher probabilities of thunderstorm development due to the presence of terrain forcing and urban–rural contrasts, especially under weakly forced large-scale environments. The Beijing metropolitan region (BMR) appears to be one such region, which is characterized by the complex topography of Mt. Yan to the north and Mt. Taihang to the west, with diverse underlying

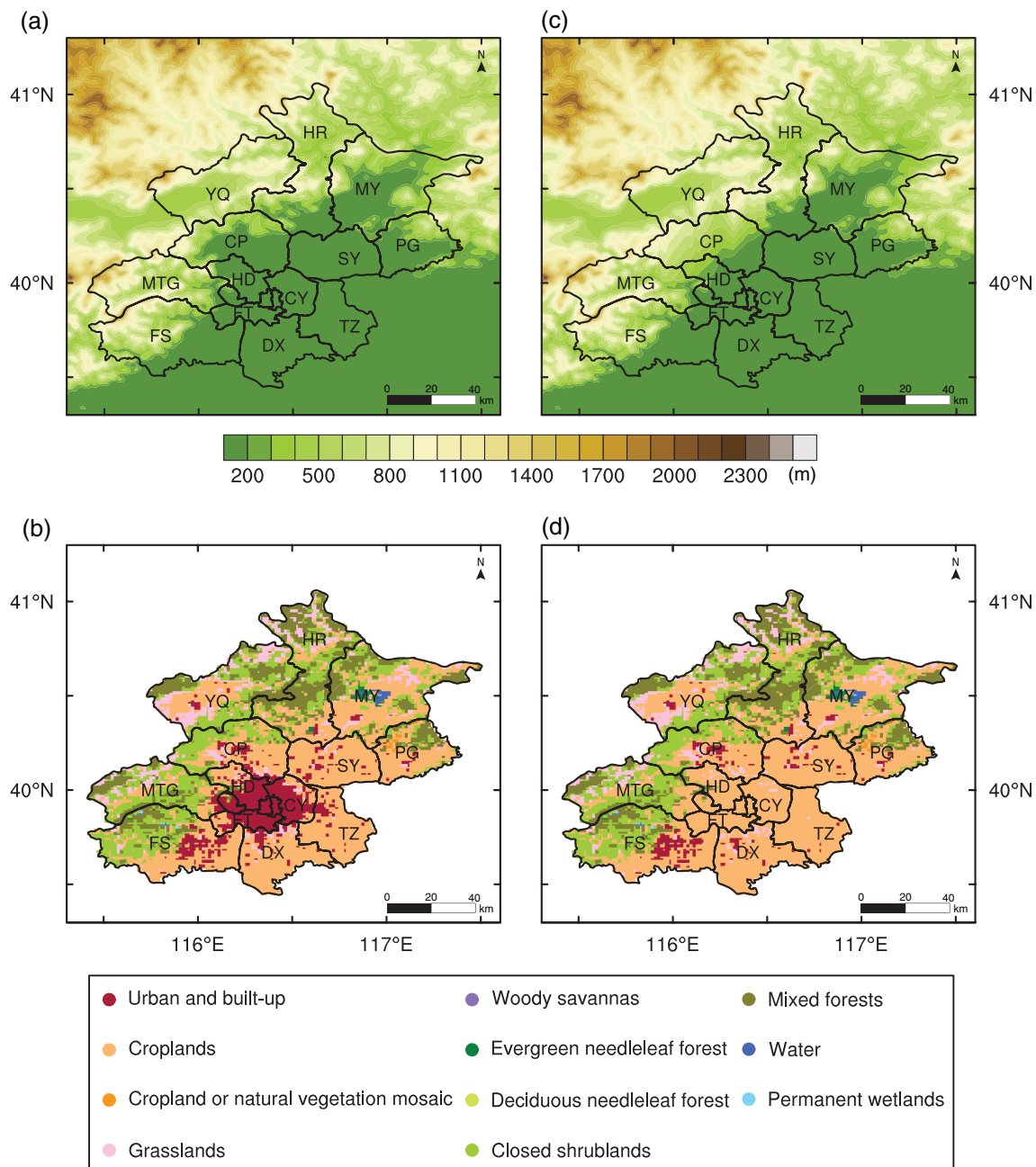


Figure 1. Terrain over the BMR for (a) the control simulation (CNTL), and (c) the simulation in which the concave valley in CP and HD is modified (Exp. NVAL; see text). Land use in the MODerate-resolution Imaging Spectroradiometer (MODIS) land use categories over the BMR used in (b) CNTL, and (d) NCUA, in which the land use over the central urban area is replaced with croplands. The BMR's Districts are abbreviated in alphabetic order as follows: CP (Changping), CY (Chaoyang), DX (Daxing), FS (Fangshan), FT (Fengtai), HD (Haidian), HR (Huairou), MTG (Mentougou), MY (Miyun), PG (Pinggu), SY (Shunyi), TZ (Tongzhou), and YQ (Yanqing); the two small Eastern and Western Districts, located to HD's immediate southeast, and Shijingshan District to HD's immediate southwest, are not denoted.

surfaces influenced by rapid urbanization (Figures 1(a) and (b)). The BMR often experiences locally generated convective storms during warm months, sometime with extreme rainfall (e.g. Sun and Yang, 2008; Chen *et al.*, 2012, 2014; Zhang *et al.*, 2013; Zhong *et al.*, 2015; Li *et al.*, 2017a).

In our previous study (i.e. Li *et al.*, 2017b, hereafter L17), we presented a successful 11 h simulation of the CI* of an isolated convective storm at the northern edge of the central urban area (CUA, consisting of Districts of Eastern, Western, Shijingshan, Haidian (HD), Chaoyang (CY), and Fengtai (FT), see Figure 1) of the BMR in the afternoon of 9 August 2011 (Figure 2(c)), hereafter referred to as the HD storm. This storm was initiated at 1600 LST (Local Standard Time = UTC + 8 h) at some distance from its northwestern mountains and two pre-existing mesoscale convective systems (MCSs) to the west and north, respectively,

and it generated heavy rainfall after merging with the western MCS (see Figs 1 and 4 in L17 for more detail). The HD storm occurred under large-scale quasi-geostrophic conditions but in a conditionally unstable regional environment in which a south-to-southeasterly flow of high- θ_e (equivalent potential temperature) air prevailed in the daytime mixed layer that was capped by an inversion (see Figs 2 and 3 in L17). This simulation is obtained using two nested grids (4/1.333 km) of Version 3.5.1 of the Weather Research and Forecasting (WRF) model. In their conceptual model, L17 hypothesize that the BMR's urban effects, the concave morphology of the BMR's western mountains (i.e. over the Changping (CP) District and HD; see Figure 1), and the convectively generated pressure perturbations to the north play different roles in determining the CI location and timing of the HD storm. Thus, the purpose of the present study is to validate the above hypothesis through a series of numerical sensitivity simulations of the effects of terrain morphology, urbanization, and the northern MCS, respectively.

*The CI is defined herein in the same manner as in L17, i.e. the appearance of the first radar echo exceeding 35 dBZ.

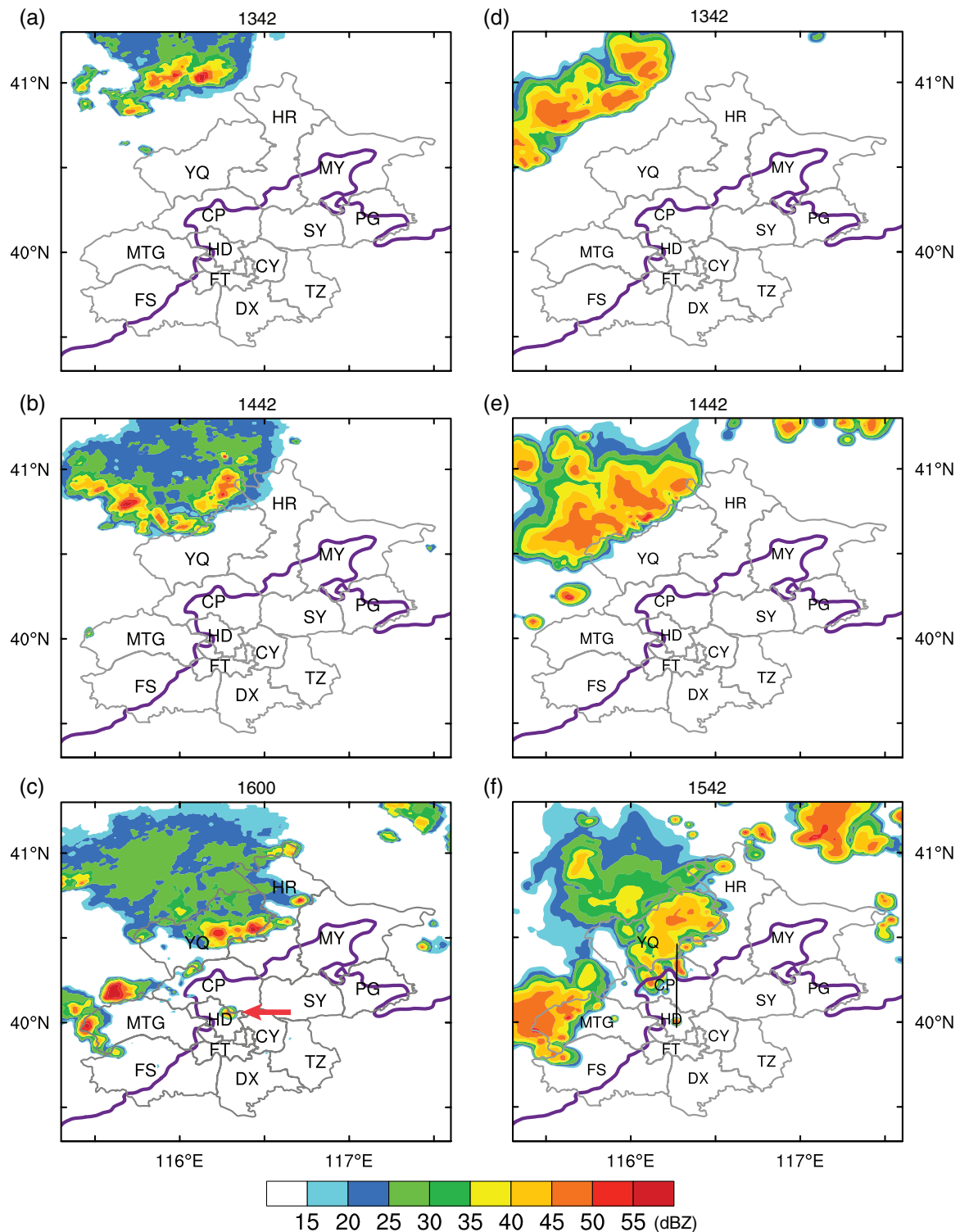


Figure 2. Radar reflectivity (dBZ) observed by Beijing's radar site at (a) 1342, (b) 1442, and (c) 1600 LST, and simulated in CNTL at (d) 1342, (e) 1442, and (f) 1542 LST 9 August 2011. A thick purple line denotes the 200 m terrain elevation; similarly for the rest of the figures. The location of the HD storm is highlighted by a red arrow in (c). A black line through HD, CP and YQ in (f) denotes the location of vertical cross-sections shown in Figure 4.

The effects of terrain forcing on the development of MCSs have long been well known. Moist flow climbing up a mountain may trigger deep convection (Caracena *et al.*, 1979; Marwitz, 1983; Rasmussen and Houze, 2011, 2016; Weckwerth *et al.*, 2014). Upslope flows and opposing ridgetop winds may form a convergence zone to the lee of a mountain, leading to CI (Banta, 1984, 1986; Banta and Schaaf, 1987). Downslope flows converging with low-level moist flow encourage the development of deep convection (Wang *et al.*, 2005; Houze, 2012). Some MCSs could be organized by local orographic flows (Cotton *et al.*, 1983; Tripoli and Cotton, 1989a, 1989b). In addition, certain terrain morphology could modulate wind direction and speed (Whiteman, 2000), thus shifting the location of convergence and

CI (Schneider and Schär, 2000; Lin *et al.*, 2001; Houze *et al.*, 2007; Romatschke *et al.*, 2010).

The urban effects on CI have become more recognized during the past two decades. Urbanization modifies the underlying surface characteristics, including roughness, soil moisture and albedo, thus affecting the location and timing of CI (Bornstein and Lin, 2000; Rozoff *et al.*, 2003; Niyogi *et al.*, 2006; Shem and Shepherd, 2009; Shepherd *et al.*, 2010). Hjelmfelt (1982) reveals that urbanization could lead to the formation of mesoscale upward motion in the PBL downwind of St. Louis. Baik *et al.* (2001) demonstrate that the urban heat island (UHI)-induced downwind updraught cell could initiate moist convection under favourable thermodynamic conditions. Baik *et al.* (2007) show

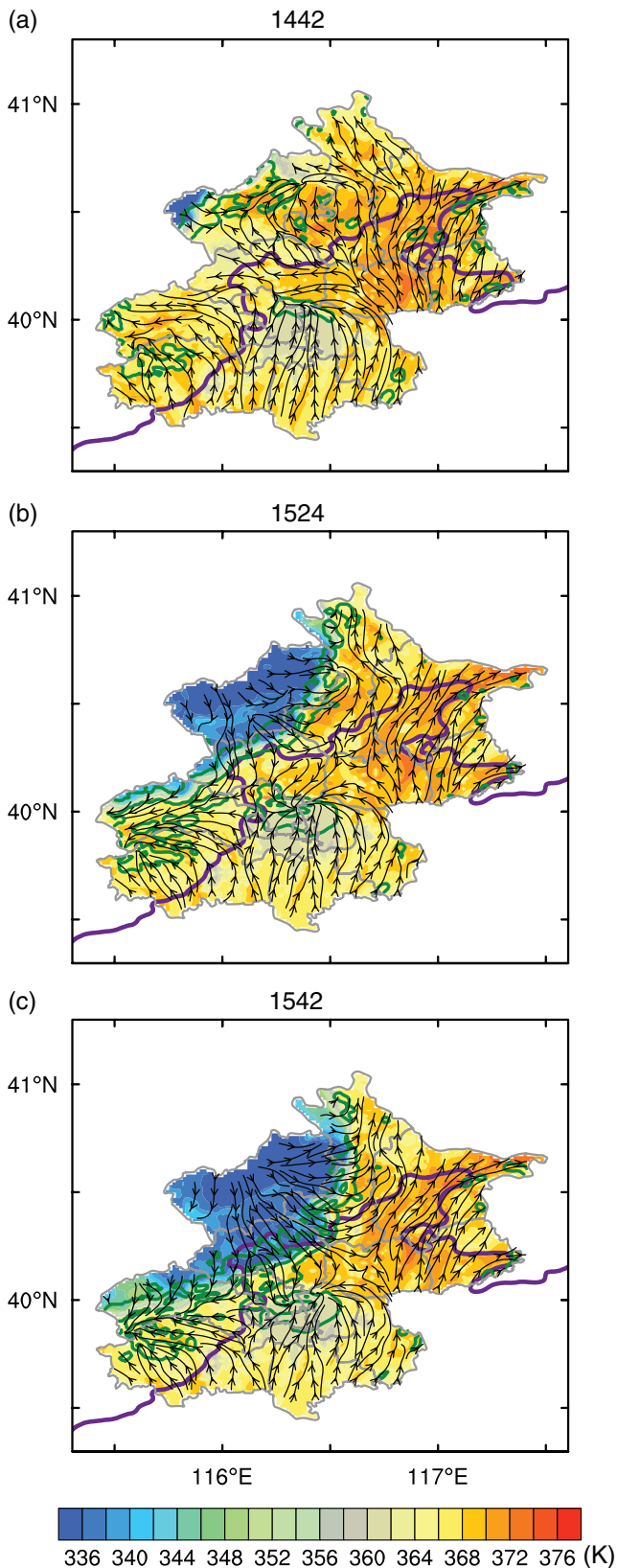


Figure 3. The simulated 2 m equivalent potential temperatures (θ_e in Kelvin, shaded) for CNTL, on which 10 m surface streamlines are superimposed, which are valid at (a) 1442, (b) 1524, and (c) 1542 LST 9 August 2011. Green contours indicate the areas of cloud condensation in the $z = 1.3\text{--}2.2$ km layer, i.e. near the top of the daytime mixed layer.

that UHI-induced circulations strengthened during the daytime could account for the formation of thunderstorms in the late afternoon or early evening. Ntelekos *et al.* (2007) find that rapid urbanization in the Baltimore metropolitan area may account for increased thunderstorm frequency as the enhanced UHI circulations interact with the Chesapeake Bay breezes. The

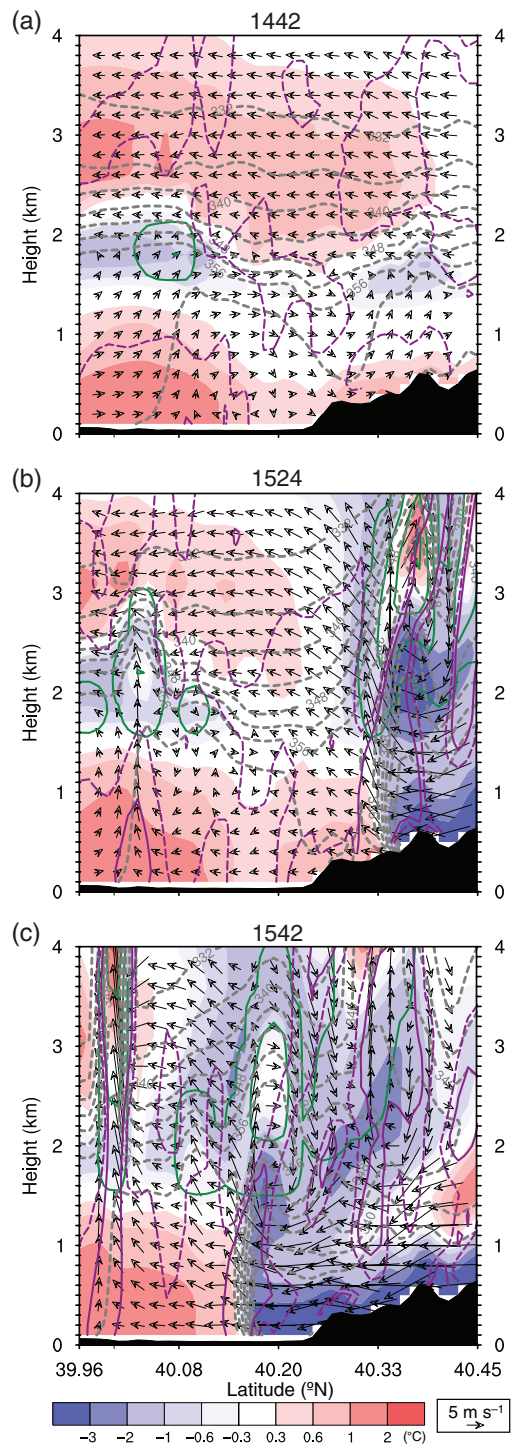


Figure 4. Vertical cross-sections for CNTL along the line given in Figure 2(f), east–west averaged over a 4 km width, of temperature perturbations from their level-averaged values (shaded, $^{\circ}\text{C}$), equivalent potential temperature (θ_e , contoured in dashed-grey at intervals of 4 K), cloud water (contoured in green starting at 0.05 g kg^{-1} at intervals of 1 g kg^{-1}), and divergence (dashed and solid magenta contours for -10^{-4} s^{-1} and -10^{-3} s^{-1} , respectively), on which in-plane flow vectors with vertical motion amplified by a factor of 5 are superimposed, which are valid at (a) 1442, (b) 1524, and (c) 1542 LST 9 August 2011. Terrain is shaded in black.

enhanced UHI circulations could also be related to upstream urbanization (Zhang *et al.*, 2009, 2011).

It has been well documented that pre-existing precipitation systems can also exert influence on the initiation and evolution of deep convection. CI may take place along cold outflow boundaries resulting from pre-existing precipitation systems (Purdum, 1976; Wilhelmson and Chen, 1982; Wilson and Schreiber, 1986; Zhang and Fritsch, 1986; Weckwerth and Wakimoto, 1992; Wilson and Mueller, 1993). Khairoutdinov and Randall (2006) design sensitivity experiments to explain the key effects of cold pools on the transition from shallow clouds to deep convection. Lima

Table 1. Description of experiment design.

Experiment	Description
CNTL	Same as Li <i>et al.</i> (2017b) but FDDA is not adopted.
NCUA	The grid points with urban and built-up land use over the central urban area are replaced with croplands.
NVAL	The terrain elevation over the concave valley in CP and HD is raised from the plain linearly to about 1000 m near the major mountain peaks to the western and northern CP.
NEVP1	Evaporative cooling is turned off at 1342 LST 9 August 2011.
NEVP2	Evaporative cooling is turned off at 1442 LST 9 August 2011.

and Wilson (2008) show that convective storms could be easily triggered by gust fronts or colliding outflow boundaries. The impact of MCSs on CI in the presence of topography involves more complicated processes. Tucker and Crook (1999) find that cold outflows from a previous MCS in the Rocky Mountains were still necessary for the CI of an MCS to the east of Denver, although surface convergence already existed at the location where the MCS developed. Bennett *et al.* (2011) and Corsmeier *et al.* (2011) demonstrate that cold outflows from a previous MCS meeting with warm and moist air over the Black Forest mountains enhanced convergence and facilitated the CI and subsequent development of an MCS.

Numerous studies have also been conducted to examine the roles of topography and urbanization in CI over the BMR during the past decade (e.g. Jiao and Bi, 2005; Sun *et al.*, 2006; Sun and Yang, 2008; Wang and Sun, 2008; Sheng *et al.*, 2012). While many previous studies have investigated the impact of terrain, urban effects and pre-existing MCSs or a combination of them on convective development, few have been performed to isolate the processes leading to the generation of isolated storms over the BMR or elsewhere, especially those that are initiated at some distance from the mountains and convectively generated outflows. Thus, in this study, we wish to address the following questions: What are the relative roles of the urbanization, terrain morphology, and remote convective forcing in governing the CI of the HD storm? Which condition determines the location and timing of the CI? These questions will be addressed through a series of sensitivity experiments.

The next section defines a control simulation (CNTL) that differs from that shown in L17. Section 3 describes the design of numerical sensitivity experiments in order to address the above questions. Section 4 presents the analyses of a series of the sensitivity simulations in relation to the CNTL. A summary and concluding remarks are given in the final section.

2. The control simulation

The model configurations used for this study are identical to those used in L17, except for the procedures to obtain the model initial conditions. Specifically, as in L17, two one-way nested grids (4/1.333 km) of the WRF model with 50 vertical levels are used in the present study. Both domains are integrated for 11 h from 0800 LST to 1900 LST 9 August 2011 with the initial and the outermost lateral boundary conditions provided by the 0.25° resolution European Centre for Medium-Range Weather Forecasts ERA-Interim data at 6 h intervals. The model physical schemes used include: (i) Rapid Radiative Transfer Model (RRTM) long-wave radiation scheme (Mlawer *et al.*, 1997); (ii) the Dudhia (1989) short-wave radiation scheme; (iii) the Morrison *et al.* (2009) double-moment microphysical parametrization; (iv) Yonsei University's PBL scheme (Hong *et al.*, 2006); and (v) a unified NOAA land-surface scheme (Chen and Dudhia, 2001). No cumulus parametrization scheme is used for either domain.

Note that L17 applies the four-dimensional data assimilation (FDDA: Stauffer and Seaman, 1990, 1994; Stauffer *et al.*, 1991) to both domains from 0800 to 1300 LST 9 August 2011 in order to

improve the quality of the model initial conditions for simulating accurately the CI location and timing of the HD storm. This implies that the free model integration in L17 begins at 1300 LST, which is about 3 h prior to the CI of the HD storm (Figure 2(c)), and less than 2 h prior to the propagation of the northern MCS into the BMR (Figure 2(b)). However, this 2–3 h period is too short to reflect the sensitivity of the model-simulated CI to the above-mentioned surface and convective forcings if this model simulation were used as a control one. Thus, a new control simulation has to be performed, termed the CNTL run, in which the same model configurations are used as those in L17 except that the FDDA procedures are turned off.

By allowing the free integration to begin at 0800 LST, the CNTL simulation could still reproduce the CI location and timing of the HD storm, but with the CI occurring about 18 min earlier and at a location that is slightly farther to the south than the observed and the previously simulated in L17. The simulated HD storm moves very slowly and it later merges with nearby storms, as observed. To see all these, Figure 2 compares the CNTL-simulated radar reflectivity to the observed, beginning at 1342 LST that is close to 6 h into the integration. Evidently, the WRF model reproduces reasonably well the northern MCS and its southeastward movement until 1442 LST (cf. Figures 2(d, e) and (a, b)). But the simulated MCS moves somewhat faster than both the observed and the L17-simulated (cf. Figures 2(c) and (f) herein and Fig. 6a in L17) during the subsequent 1 h period, i.e. at 1542 LST when the CI of the HD storm occurs. Similarly, the WRF model reproduces reasonably well the MCS over the BMR's western mountains, albeit a little stronger than the observed (cf. Figures 2(f) and (c)).

Despite the differences, it is encouraging that the WRF-simulated CI location and timing are about 10 km to the south of the observed location and 18 min earlier than the observed, respectively. L17 have hypothesized that the northern MCS plays some role in the CI of the HD storm due to the presence of significant cold outflows with meso-high pressures (see Fig. 12 therein), whereas the western MCS affects the CI little, due to the absence of a pronounced cold pool at that time. Thus, in the analysis that follows, we will pay more attention to the impact of the northern MCS on the CI of the HD storm.

After analysing surface observations and model-simulation results, L17 find that the growth of the mixed layer, aided by the UHI effects, accounts for the formation of a thin layer of cloud condensation at the top of the PBL at the CI site. To facilitate the comparison of the control run to the sensitivity simulations to be described below, Figures 3 and 4 present the surface-layer θ_e and streamlines, and vertical cross-sections of θ_e , temperature perturbations and in-plane flow vectors as well as grid-box saturation during the 1 h period prior to CI, respectively. We can see a southerly flow of high- θ_e air (i.e. 362–368 K) that converges with an easterly flow of higher- θ_e air (i.e. >368 K), leading to the formation of upward motion (as implied by intersecting streamlines), a distinctly deeper mixed layer, and grid-box saturation near the top of the mixed layer around the HD–CP border (Figures 3(a) and 4(a)). Note that the cloud condensation occurs at about 1 h prior to CI, i.e. the appearance of the first radar echo (cf. Figures 3(a) and 2(f)), since the latter is an indication of precipitation. The concave valleys in the BMR's western mountains help shift the incoming southerly flow westward to facilitate the formation of the convergence area near the HD–CP border. Meanwhile, the convectively generated cold pool associated with the northern MCS begins to enter the BMR at 1442 LST (cf. Figures 2(e) and 3(a)), and reaches the 200 m terrain elevation by 1542 LST (cf. Figures 2(f) and 3(c)).

Of importance is that the north-to-northwesterly surface flows extend into the area of higher- θ_e air, i.e. significantly ahead of the cold pool, and then converge toward the CI site with the southerly and easterly flows near the HD–CP border (Figures 3(b) and (c)). The flows of higher- θ_e surface air appear to be attributable partly to the pressure gradient force of a meso- β -scale high associated with the northern MCS (see L17), and

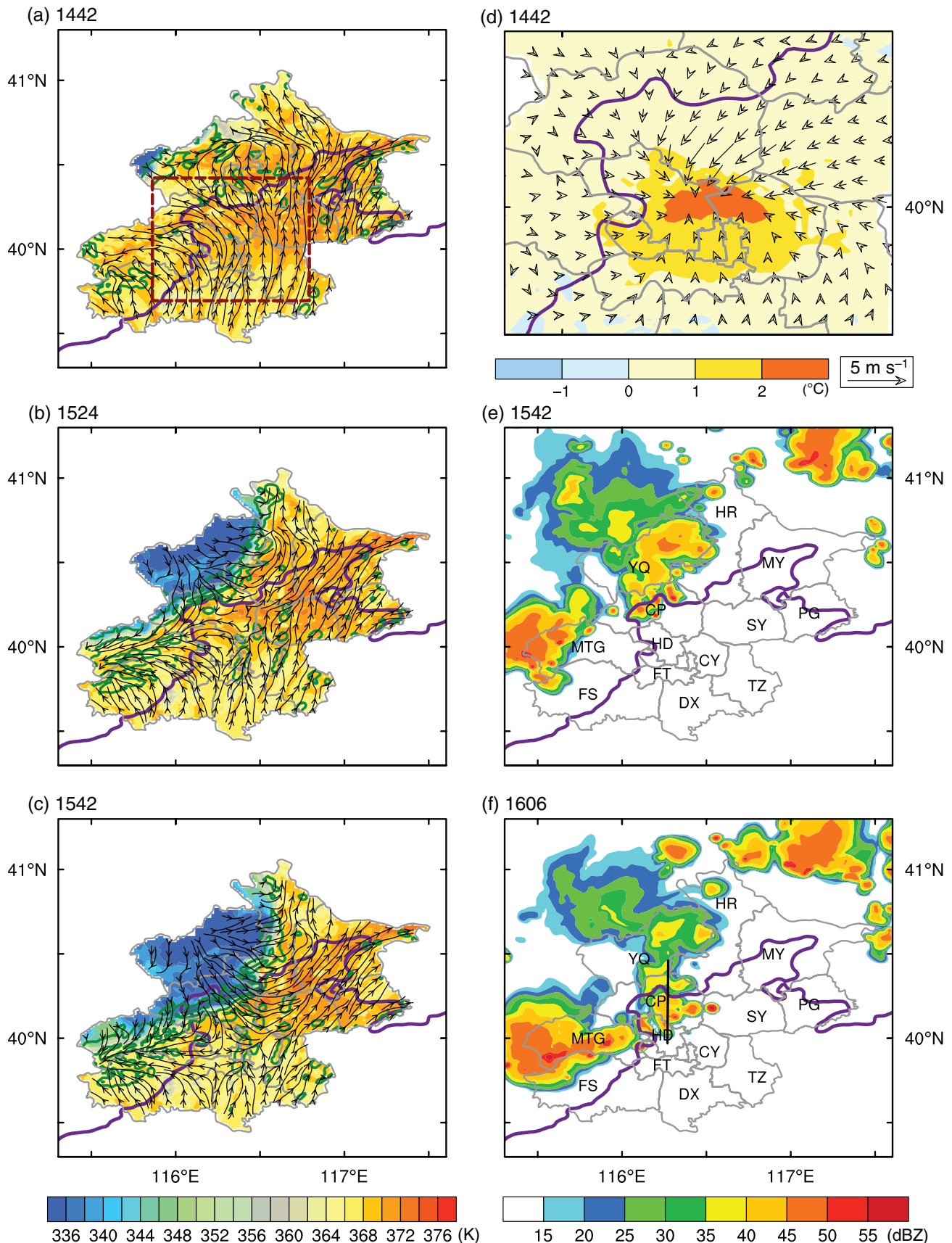


Figure 5. As in Figure 3 but for Exp. NCUA at (a) 1442, (b) 1524, and (c) 1542 LST 9 August 2011. The red-dashed rectangle in (a) denotes the subdomain used in (d) showing the differed fields of 2 m temperature ($^{\circ}\text{C}$, shaded), and 10 m surface winds between CNTL and NCUA (i.e. CNTL – NCUA) at 1442 LST. As in Figure 2 but for Exp. NCUA at (e) 1542, and (f) 1606 LST 9 August 2011. A black line in (f) denotes the location of vertical cross-sections shown in Figure 6.

partly to the presence of latent heat release associated with grid-box saturation near the PBL top at the CI site (Figures 4(b) and (c)). As a result, cloud condensation expands in coverage and depth (Figures 3(b), (c) and 4(b), (c)). At the time of CI, the cloud condensation has spread over a pronounced area in the HD, CP and CY districts, whereas the associated radar

reflectivity just begins to emerge. An organized condensation band also takes place along the leading edge of the cold outflow boundaries, as can be expected. It is apparent that the HD storm is initiated much ahead of the cold outflow boundaries, implying that it is not directly triggered by any of the pre-existing MCSs.

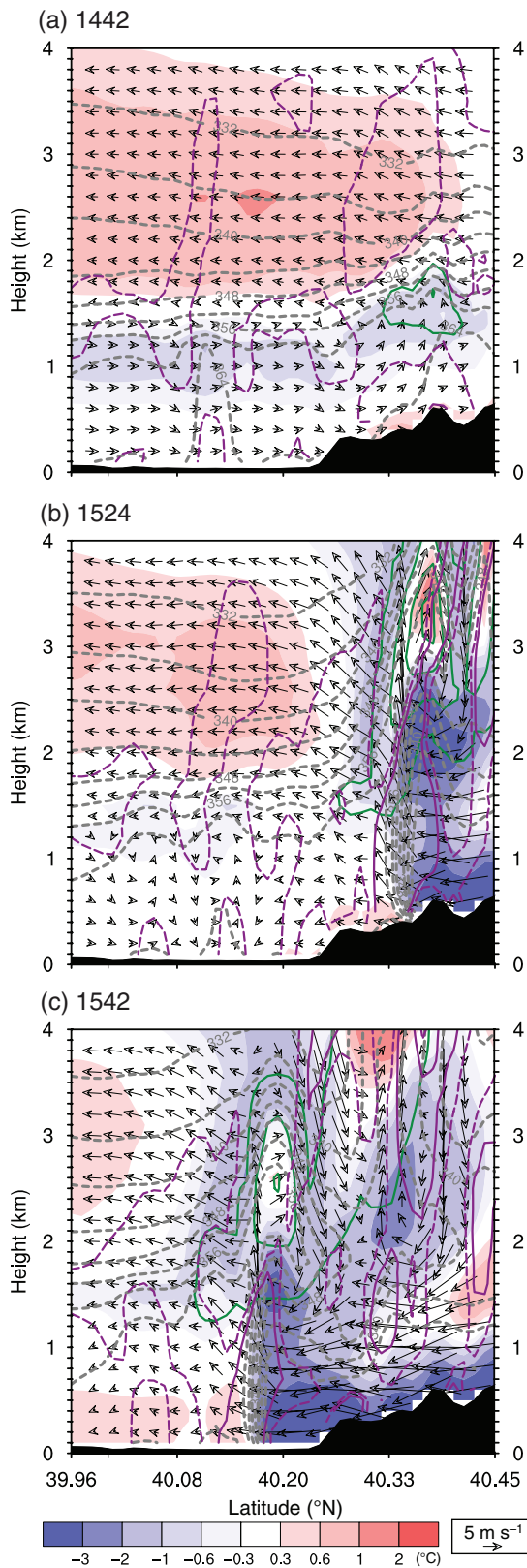


Figure 6. (a–c) As in Figure 4 but for Exp. NCUA. Vertical cross-sections are taken along the line given in Figure 5(f).

3. Experiment design

In view of the different roles of urbanization, terrain morphology, and remote convective forcing (i.e. the northern MCS) in the CI of the HD storm, several sensitivity experiments are performed (see Table 1), in which all the model parameters are identical to those in CNTL, except that one of the above features is turned off or modified. For example, to test the impact of urbanization on the CI of the HD storm, the urban and built-up land use over the CUA of the BMR is replaced by croplands that are the

same as those over the neighbouring rural region (cf. Figures 1(b) and (d)), hereafter referred to as experiment (Exp.) NCUA. This procedure will alter the surface energy budget over the urban region through reduced roughness, increased evaporation of soil moisture, and albedo, thereby removing the urban effects and limiting the growth of the daytime mixed layer.

Experiment NVAL is conducted to examine to what extent the ‘concave valley’ affects the cyclonic turning of the larger-scale southerly flows and the CUA-induced easterly flow as well as later northerly flow associated with the northern MCS. This is done by raising the elevation of the ‘concave valley’ over CP and HD from 200 m at the western edge of the plain linearly to about 1000 m near the major mountain peak to the western and northern CP (Figure 1(c)).

The influences of convectively generated cold outflows associated with the northern MCS on the CI of the HD storm are explored by showing two sensitivity experiments, in which evaporation of rainwater is allowed when meeting with dry air (i.e. as in CNTL) but the associated evaporative cooling in the thermodynamic equation is turned off at two different stages of the northern MCS with different distances between MCS and HD. Specifically, the above options are activated after 1342 and 1442 LST, hereafter referred to as Exps. NEVP1 and NEVP2, respectively, when the northern MCS is located far from and near the northwestern border of the BMR (Figures 2(d) and (e)). At 1342 LST, the PBL top reaches over 1 km altitude with little evidence of grid-box saturation (not shown), whereas the grid-box saturation just occurs at 1442 LST (e.g. Figure 4(a)). Thus, the two simulations will be used to show to what extent the evaporative-driven cold outflows associated with the northern MCS impact on the timing of the grid-box saturation at the mixed-layer top and on the CI of the HD storm.

4. Results

In this section, the results from the sensitivity simulations described in the preceding section are examined to gain insight into the relative contributions of urbanization, mountain morphology, and the northern MCS to the CI of the HD storm.

4.1. Effects of urbanization

By replacing the CUA land use with that of croplands (Exp. NCUA), the model produces a quite different surface flow pattern around the ‘CUA’ from that in CNTL (cf. Figures 5 and 3). That is, surface streamlines exhibit southerly flows over all the districts on the east of the ‘CUA’, with little evidence of converging easterly flows. Only part of the southerly flow through and to the west of the ‘CUA’ turns to a southeasterly up-valley flow through the concave valley in the western mountains. Of significance is that the peak mixed-layer depth at the ‘CP’ site could only reach 1.2 km altitude, as compared to a distinct depth of 1.8 km in CNTL (cf. Figures 6(a) and 4(a)), due partly to the lacking low-level convergence (and lifting), and partly to the absence of the UHI effects. As a result, the PBL top cloud formation in NCUA is markedly delayed, as expected, with sporadic grid-box saturation at only a few points. This indicates the important role of the developing easterly flow in the CI of the CNTL-HD storm. More significant cloud formation takes place at later times as a result of the further growth of the mixed layer (Figures 5(b) and (c)).

Of interest is that removing the CUA eliminates most of the surface ‘high- θ_e outflows’ from its northwest (cf. Figures 5(b), (c) and 3(b), (c)), suggesting that the ‘outflows’ in CNTL are at least not entirely convectively generated by the northern MCS, but represent the ‘converging inflows in the PBL’ of the incipient HD storm due to diabatic heating near the PBL top. Of course, this should not be considered as the direct but the indirect impact of the CUA through its induced diabatic heating near the PBL top. Even at 1542 LST, the cloud-condensation layer still remains shallow and the first radar echo associated with

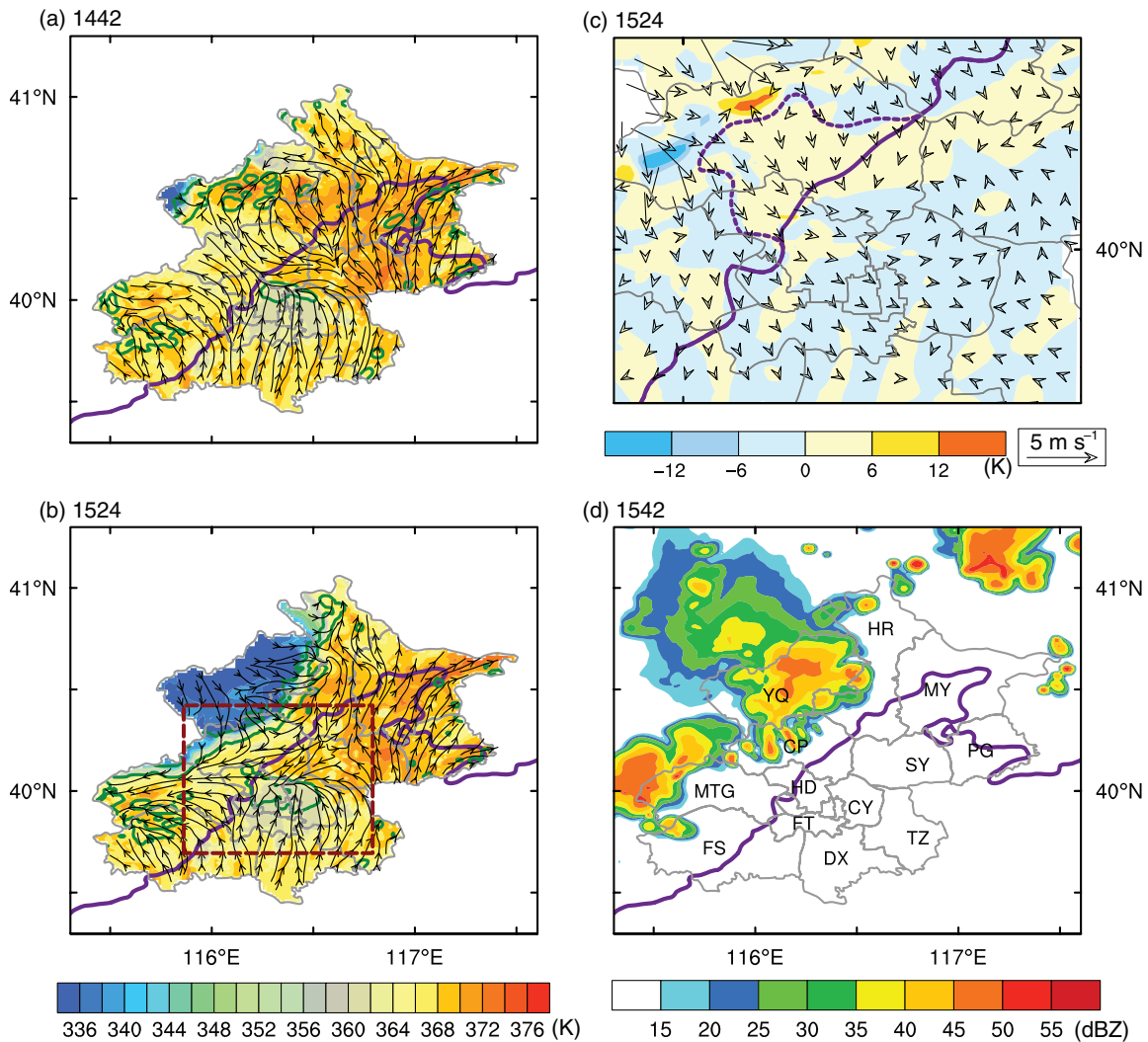


Figure 7. As in Figure 3 but for Exp. NVAL at (a) 1442 LST, and (b) 1524 LST. The red-dashed rectangle in (b) denotes the subdomain used in (c) showing the differenced fields of 2 m equivalent potential temperature (θ_e , K, shaded), and 10 m surface winds between CNTL and NVAL (i.e. CNTL – NVAL) at 1524 LST. A purple-dashed line denotes the original 200 m terrain elevation in Exp. CNTL and a purple-solid line denotes the modified 200 m terrain elevation in Exp. NVAL. (d) As in Figure 2, but for Exp. NVAL at 1524 LST.

the HD storm has not developed (Figures 5(c) and (e)). A few localized storms begin to appear after 1600 LST (Figure 5(f)), as a result of the approaching cold outflow boundaries, as can be extrapolated from the secondary circulation shown in Figure 6(c). The above results confirm the important contribution of the CUA to the CI of the HD storm. On the other hand, the northern MCS influences its ambient flows beyond cold outflow boundaries, especially in the low troposphere, as can be seen from Figures 4(b), (c) and 6(b), (c) showing the generation of upward motion, and the PBL-top condensation to the south, like the surface outflows ahead of the convectively generated cold pools (Figures 3(b), (c) and 5(b), (c)).

Of interest to note is that removing the CUA allows for the generation of cloud-condensation bands in the southerly flows in the late afternoon when the mixed layer is well developed (Figures 5(b) and (c)). These cloud bands are similar to roll vortices in the PBL as discussed by LeMone (1973), Moeng and Sullivan (1994), and Young *et al.* (2002), and they are generated by the vertical wind shear in the PBL. They do not appear in CNTL (cf. Figures 5(c) and 3(c)), because the presence of the CUA facilitates convergence of the incoming southerly flows (and moisture) and divergent flows around it to the east such that local grid-box saturation near the PBL top occurs much earlier than that in NCUA.

Two mechanisms, i.e. the UHI and ‘blocking’ effects, could be used to explain why the presence of the CUA facilitates the development of a southeasterly-to-easterly flow over its eastern parts, and of low-level convergence and increased PBL depth

near the CI site. First, when the CUA’s urban land is replaced by croplands that are the same as those in the nearby rural regions, the UHI effect is eliminated. This results in little near-surface temperature contrast and little flow inhomogeneity between the CUA and its rural areas. When the UHI effects in the CUA are imposed in Exp. CNTL, an urban circulation with the warmer air rising over the CUA and the surrounding air converging towards the CUA takes place, as shown by the differenced surface flows and temperatures (i.e. CNTL – NCUA) in Figure 5(d). A similar converging flow pattern was also shown on the downwind side of Atlanta (Bornstein and Lin, 2000), and St. Louis (Rozoff *et al.*, 2003).

The ‘blocking’ effects of the CUA can be clearly seen from the northerly differenced surface flows that are more pronounced in the north (Figure 5(d)). In the absence of the CUA, the southerly air moves across the CUA until hitting the foothills where a directional shift to southeasterly occurs (Figure 5(a)), whereas the southerly flow is obstructed at the CUA in Exp. CNTL. This could also be clearly seen from Figure 5(d) showing more pronounced northeasterly (differenced) flows on the downwind side. Note that although the ‘blocking’ effects by buildings are not explicitly represented, as either in a single-layer or a multi-layer urban canopy model (Kusaka *et al.*, 2001; Martilli *et al.* 2002), they are parametrized by the associated frictional effects through increased roughness lengths in the unified NOAH land-surface scheme (Chen and Dudhia, 2001). Numerous studies have shown the impacts of increased surface roughness over an urban area on modifying surface meteorological conditions (e.g. Huff and

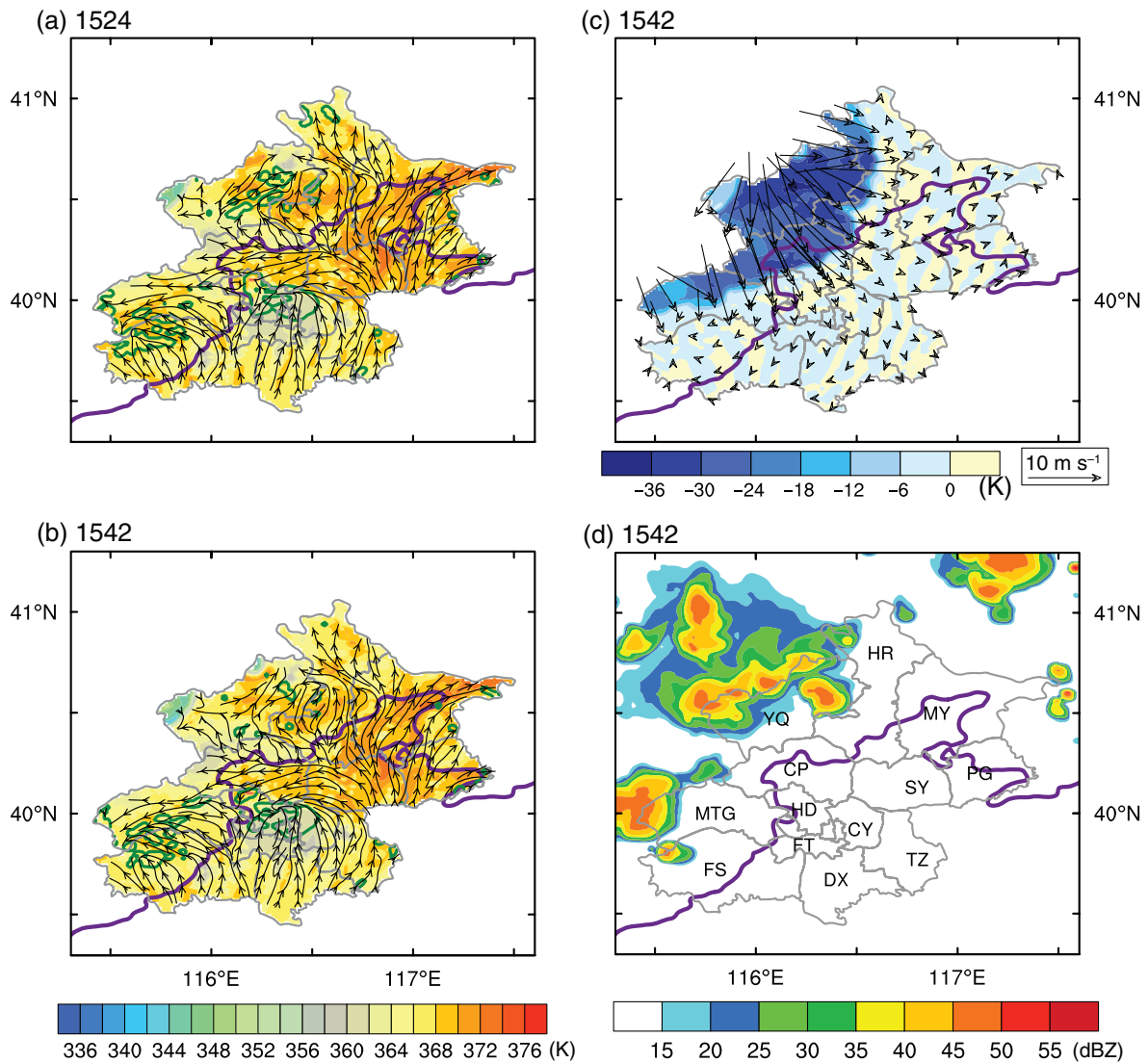


Figure 8. As in Figure 3, but for Exp. NEVP1 at (a) 1524, and (b) 1542 LST. (c) The differenced fields of 2 m equivalent potential temperature (θ_e , K, shaded), and 10 m surface winds between CNTL and NEVP1 (i.e. CNTL – NEVP1) at 1542 LST. (d) As in Figure 2, but for Exp. NEVP1 at 1542 LST.

Vogel, 1978; Hjelmfelt, 1982; Thielen *et al.*, 2000). As a result of both the UHI- and dynamically-induced convergence, the PBL depth at the CI site grows faster than that in the nearby rural regions (Figure 4(a)). Thus, in the absence of the CUA, the PBL depth over HD remains as shallow as that in the rural regions (cf. Figures 4(a) and 6(a)), and CI cannot take place, due to the lack of additional surface heating and lifting, until the cold outflow associated with the MCS arrives (Figure 5(f)).

4.2. Effects of terrain morphology

Eliminating the ‘northwestward-concave valley’ in Exp. NVAL results in subtle changes in the cyclonic turning of southerly flows near the CI site at 1442 LST (Figure 7(a)). This appears to be attributable mainly to the dominance of a low-level cyclonic circulation (see Figs 2b,c in L17), and secondarily to the mass convergence induced by latent heat release associated with the western MCS and cloud condensation near the PBL top over the southwestern mountains.

However, eliminating the concave valley reduces the northerly ‘outflow’ component ahead of the convectively generated cold pool at 1524 LST when the latter approaches the 200 m terrain contour (Figure 7(b)). Instead, the up-valley surface streamlines diverge around the leading edge of the cold pool in Exp. NVAL, as compared to the divergent northwesterly flows that are normal to the cold pool and sharply downslope in Exp. CNTL (cf. Figures 7(b) and 3(b)). These differences in the surface flows are more evident from the differenced flow field, given in Figure 7(c),

showing organized convergence (in CNTL) towards the CI site in HD. As a result of the reduced low-level convergence from the northwesterly flow in NVAL, the HD storm fails to form even at 1542 LST (Figure 7(d)), despite the formation of a well-defined coverage of cloud condensation near the PBL top as induced by the CUA (Figure 7(b)). The CI of the storm in HD does not occur until 1600 LST when the cold outflow boundaries arrive at the CI site (not shown).

4.3. Effects of evaporative-driven cold outflows

Given the importance of cold outflows in assisting the formation of the HD storm, two different timings of the approaching cold outflows of the northern MCS are demonstrated. In the first experiment, evaporative cooling is turned off at the time when the northern MCS is far away from the BMR’s northwestern border, i.e. at 1342 LST (Exp. NEVP1). This procedure leads to the absence of a distinct cold pool over the northwestern mountainous regions in the BMR despite the presence of deep convection (Figure 8). Because of the absence of the associated cold outflows, surface flows over the western mountains are still dominated by up-valley motions ranging from southeasterly to easterly and southwesterly even by 1542 LST (Figures 8(a) and (b)), indicating the importance of the convectively generated cold domes in generating the divergent north-to-northwesterly outflows, as demonstrated in the differenced flows given in Figure 8(c). In particular, we can infer from Figure 8(c) the lack of north-to-northwesterly flows through the concave valley in

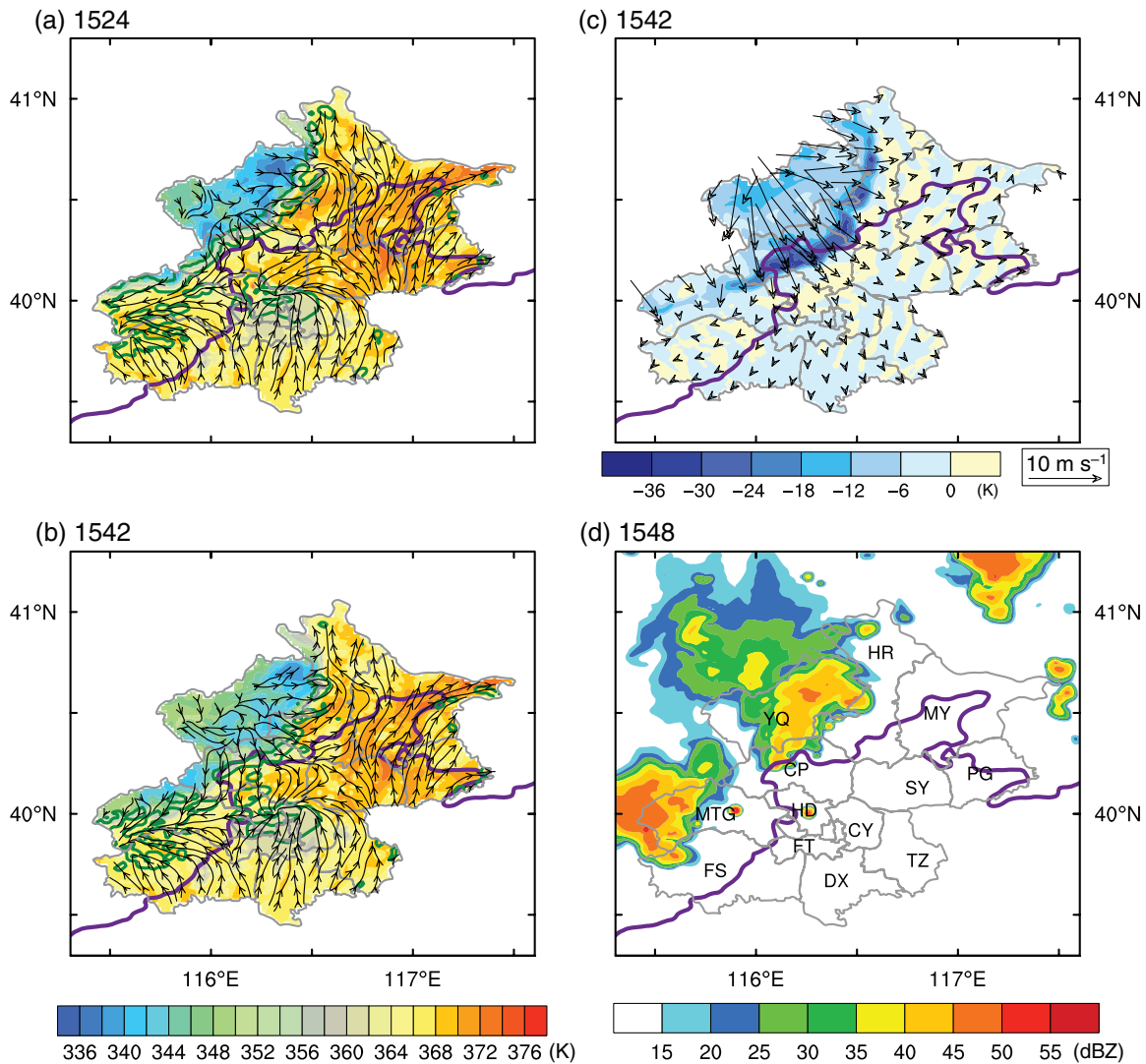


Figure 9. As in Figure 3 but for Exp. NEVP2 at (a) 1524, and (b) 1542 LST. (c) The differenced fields of 2 m equivalent potential temperature (θ_e , K, shaded), and 10 m surface winds between CNTL and NEVP2 (i.e. CNTL – NEVP2) at 1542 LST. (d) As in Figure 2 but for Exp. NEVP2 at 1548 LST.

NEVP1, which in turn reduce the low-level convergence near the CI site. Thus, the HD storm fails to develop even by 1542 LST (Figure 8(d)) and 1600 LST (not shown), even though cloud condensation still takes place near the mixed-layer top as it does in CNTL. This indicates again that the CUA-related UHI effects and urban-induced low-level convergence alone could not be strong enough to break through the stable layer above. This result also helps explain why the western MCS moves slowly eastward and affects the formation of the HD storm little, as mentioned in L17, due to the lack of a convectively generated cold pool during the early stages.

In the second experiment (Exp. NEVP2), evaporation cooling is turned off at the time when the leading cold outflows of the northern MCS arrive at the BMR's northwestern border at 1442 LST (Figure 2(e)). A comparison of Figures 9(a), (b) and 3(b), (c) shows the presence of a relatively weaker cold pool with weaker northerly flows through the concave valley in NEVP2, while the cloud condensation coverage near the PBL top at the CI site still remains similar to that in CNTL. However, the cold pool in NEVP2 is stronger than that in NEVP1 (cf. Figure 9(b), (c) and 8(b), (c)). Thus, CI of the HD storm occurs in NEVP2, as compared to its absence in NEVP1, but it does not take place until 1548 LST (Figure 9(d)), which is a few minutes later than that in CNTL. Again, the CI of the HD storm is accompanied with pronounced northerly flows through the concave valley (cf. Figures 9(b) and (d)). This result confirms further the importance of the northerly flows through the concave valley associated with the convectively generated cold pool of the northern MCS in the CI of the HD storm.

5. Summary and conclusions

In this study, a series of numerical experiments is performed based on the results presented in L17 in order to investigate the different effects of the CUA, terrain morphology, and remote convective forcing on the location and timing of the CI of an isolated thunderstorm near the HD District. Results confirm the hypothesis put forward by L17 that the CUA, a mesoscale concave valley in the BMR's western mountains, and an approaching MCS from the northwestern mountainous region contribute in different degrees to the CI of the HD storm, which are summarized below.

The CUA plays an important role in facilitating the growth of the daytime mixed layer and the generation of cloud condensation near the mixed-layer top due to increased surface sensible heat fluxes (i.e. the UHI effects) and the UHI-induced convergence as well as increased frictional convergence (i.e. the CUA's 'blocking' effects). The collective effects shift southerly flows to southeast-to-easterly flows on the CUA's east side. In the absence of the CUA, the shallow clouds near the mixed-layer top develop at a time much later than that in CNTL, and the HD storm does not take place until the arrival of cold outflow boundaries associated with the northern MCS.

The 'northwestward concave valley' in the BMR's western mountains facilitates southeasterly up-valley flows during the daytime without any convective influence in the present case. It tends to induce northerly downslope flows far ahead of the cold outflow boundaries of the northern MCS, thereby enhancing the low-level convergence near the CI site. CI of the HD storm

could not take place in any simulation in which no pronounced northerly flows through the concave valley are present.

The northern MCS influences the timing and location of CI of the HD storm by producing cold outflows with meso-high pressures, which tends to induce upward motion far ahead and northerly downslope flows through the concave valley as the associated cold pool enters the northwestern mountains. When evaporative cooling is turned off at different stages of the northern MCS, the position and strength of meso-high pressures and cold outflows vary, so do the strength of northerly flows through the concave valley that are driven by the meso-high pressures. If evaporative cooling is turned off when the northern MCS is far away from the BMR's border, surface flows over the western mountains are dominated by up-valley motions and little northerly flow occurs through the concave valley. The HD storm does not develop in spite of well-developed cloud condensation near the mixed-layer top. In contrast, the HD storm does occur, albeit a few minutes later than that in CNTL, if evaporative cooling is turned off after the northern MCS moves across the BMR's northwestern border, because of the presence of significant northerly flows through the concave valley.

In conclusion, we may state that the UHI and friction-induced low-level convergence of the CUA plays an important role in preconditioning the pre-storm environment of the HD storm, and it is the approaching cold outflows of the northern MCS that induce northerly downslope flows through the concave valley to enhance the low-level convergence, leading to the CI of the HD storm. Previous statistical studies using radar data (Chen *et al.*, 2012, 2014) and surface observations (Li *et al.*, 2017a) show that the HD-CP border region is vulnerable to convective storms and heavy rainfall, especially during the afternoon and evening hours. The results in this study have important implications for the understanding and prediction of CI of these storms. The important role of the northerly flows in CI suggests that the forecasters should pay more attention to the change of wind direction to the north of the urban area when southerly or southeasterly winds prevail over the plain. More observation instruments, e.g. wind profilers, are expected to be constructed to the north of the urban area. In addition, this study helps advance the understanding of heavy rainfall formation over and on the downstream side of any urban area of a megacity. The most recent example was a record-breaking rainfall event with up to 524 mm accumulated rainfall in 12 h and the maximum hourly rainfall rate of 180 mm h⁻¹ that occurred on 7 May 2017 on the downstream side of Guangzhou, a megacity in south China. Clearly, more observational and modelling case-studies are needed to investigate the roles of multi-scale interactions of various forcing types, including urban-rural circulations and topography, in the frequent CIs of heavy-rain-producing thunderstorms during the summer season over the BMR and elsewhere.

Acknowledgments

This work was supported by the National Basic Research Program of China (973 Program) under grant No. 2014CB441402. The authors are grateful to the Beijing Meteorological Bureau for providing observational data in the BMR. The model simulations were performed on TianHe-1 (A) at the National Supercomputer Center in Tianjin, China. The first author is also grateful to the UCAS Joint PhD Training Program, which allowed her to complete this article in the Department of Atmospheric and Oceanic Science, University of Maryland.

References

Baik JJ, Kim YH, Chun HY. 2001. Dry and moist convection forced by an urban heat island. *J. Appl. Meteorol.* **40**: 1462–1475.
 Baik JJ, Kim YH, Chun HY. 2007. Effects of boundary-layer stability on urban heat island-induced circulation. *Theor. Appl. Climatol.* **89**: 73–81.
 Banta RM. 1984. Daytime boundary layer evolution over mountainous terrain. Part I: Observations of the dry circulations. *Mon. Weather Rev.* **112**: 340–356.

Banta RM. 1986. Daytime boundary layer evolution over mountainous terrain. Part II: Numerical studies of upslope flow duration. *Mon. Weather Rev.* **114**: 1112–1130.
 Banta RM, Schaaf CB. 1987. Thunderstorm genesis zones in the Colorado Rocky Mountains as determined by traceback of geosynchronous satellite images. *Mon. Weather Rev.* **115**: 463–476.
 Bennett LJ, Blyth AM, Burton RR, Gadian AM, Weckwerth TM, Behrendt A, Di Girolamo P, Dorninger M, Lock SJ, Smith VH, Mobbs SD. 2011. Initiation of convection over the Black Forest mountains during COPS IOP 15a. *Q. J. R. Meteorol. Soc.* **137**: 176–189.
 Bornstein R, Lin Q. 2000. Urban heat islands and summertime convective thunderstorms in Atlanta: Three case studies. *Atmos. Environ.* **34**: 507–516.
 Caracena F, Maddox RA, Hoxit LR, Chappell CF. 1979. Mesoanalysis of the Big Thompson storm. *Mon. Weather Rev.* **107**: 1–17.
 Chen F, Dudhia J. 2001. Coupling an advanced land surface-hydrology model with the Penn State-NCAR MM5 modeling system. Part I: Model description and implementation. *Mon. Weather Rev.* **129**: 569–585.
 Chen M, Wang Y, Gao F, Xiao X. 2012. Diurnal variations in convective storm activity over contiguous north China during the warm season based on radar mosaic climatology. *J. Geophys. Res.* **117**: D20115. <https://doi.org/10.1029/2012JD018158>.
 Chen M, Wang Y, Gao F, Xiao X. 2014. Diurnal evolution and distribution of warm-season convective storms in different prevailing wind regimes over contiguous north China. *J. Geophys. Res.* **119**: 2742–2763. <https://doi.org/10.1002/2013JD021145>.
 Corsmeier U, Kalthoff N, Barthlott C, Aoshima F, Behrendt A, di Girolamo P, Dorninger M, Handwerker J, Kottmeier C, Mahlke H, Mobbs SD, Norton EG, Wickert J, Wulfmeyer V. 2011. Processes driving deep convection over complex terrain: a multi-scale analysis of observations from COPS IOP 9c. *Q. J. R. Meteorol. Soc.* **137**: 137–155.
 Cotton WR, George RL, Wetzell PJ, McAnelly RL. 1983. A long-lived mesoscale convective complex. Part I: The mountain-generated component. *Mon. Weather Rev.* **111**: 1893–1918.
 Dudhia J. 1989. Numerical study of convection observed during the winter monsoon experiment using a mesoscale two-dimensional model. *J. Atmos. Sci.* **46**: 3077–3107.
 Fritsch JM, Chappell CR. 1980. Numerical prediction of convectively-driven mesoscale pressure systems. Part I: Convective parameterization. *J. Atmos. Sci.* **37**: 1722–1733.
 Hjelmfelt MR. 1982. Numerical simulation of the effects of St. Louis on mesoscale boundary-layer airflow and vertical air motion: Simulations of urban vs non-urban effects. *J. Appl. Meteorol.* **21**: 1239–1257.
 Hong SY, Noh Y, Dudhia J. 2006. A new vertical diffusion package with an explicit treatment of entrainment processes. *Mon. Weather Rev.* **134**: 2318–2341.
 Houze RA Jr. 2012. Orographic effects on precipitating clouds. *Rev. Geophys.* **50**: RG1001. <https://doi.org/10.1029/2011RG000365>.
 Houze RA Jr, Wilton DC, Smull BF. 2007. Monsoon convection in the Himalayan region as seen by the TRMM precipitation radar. *Q. J. R. Meteorol. Soc.* **133**: 1389–1411.
 Huff FA, Vogel JL. 1978. Urban, topographic and diurnal effects on rainfall in the St. Louis region. *J. Appl. Meteorol.* **17**: 565–577.
 Jiao M, Bi B. 2005. Mesoscale structure analysis of topography-induced heavy rainfall in Beijing in summer. *Meteorol. Mon.* **31**: 9–14 (in Chinese with English Abstract).
 Johns RH, Doswell CA III. 1992. Severe local storms forecasting. *Weather and Forecasting* **7**: 588–612.
 Johnson RH, Mapes BE. 2001. Mesoscale processes and severe convective weather. In *Severe Convective Storms*, III Doswell CA. (ed.): 71–122. American Meteorological Society: Boston, MA.
 Kain JS. 2004. The Kain-Fritsch convective parameterization: an update. *J. Appl. Meteorol.* **43**: 170–181.
 Khairoutdinov M, Randall D. 2006. High-resolution simulation of shallow-to-deep convection transition over land. *J. Atmos. Sci.* **63**: 3421–3436.
 Kusaka H, Kondo H, Kikegawa Y, Kimura F. 2001. A simple single-layer Urban Canopy Model for atmospheric models: Comparison with multi-layer and slab models. *Boundary-Layer Meteorol.* **101**: 329–358.
 LeMone MA. 1973. The structure and dynamics of horizontal roll vortices in the planetary boundary layer. *J. Atmos. Sci.* **30**: 1077–1091.
 Li H, Cui X, Zhang DL. 2017a. A statistical analysis of hourly heavy rainfall events over the Beijing metropolitan region during the warm seasons of 2007–2014. *Int. J. Climatol.* **37**: 4027–4042. <https://doi.org/10.1002/joc.4983>.
 Li H, Cui X, Zhang DL. 2017b. On the initiation of an isolated heavy-rain-producing storm near the central urban area of Beijing metropolitan region. *Mon. Weather Rev.* **145**: 181–197.
 Lima MA, Wilson JW. 2008. Convective storm initiation in a moist tropical environment. *Mon. Weather Rev.* **136**: 1847–1864.
 Lin YL, Chiao S, Wang TA, Kaplan ML, Weglarz RP. 2001. Some common ingredients for heavy orographic rainfall. *Weather and Forecasting* **16**: 633–660.
 Martilli A, Clappier A, Rotach MW. 2002. An urban surface exchange parameterization for mesoscale models. *Boundary-Layer Meteorol.* **104**: 261–304.

- Marwitz JD. 1983. The kinematics of orographic airflow during Sierra storms. *J. Atmos. Sci.* **40**: 1218–1227.
- Mlawer EJ, Taubman SJ, Brown PD, Iacono MJ, Clough SA. 1997. Radiative transfer for inhomogeneous atmosphere: RRTM, a validated correlated-k model for the longwave. *J. Geophys. Res.* **102**: 16663–16682. <https://doi.org/10.1029/97JD00237>.
- Moeng CH, Sullivan PP. 1994. A comparison of shear- and buoyancy-driven planetary boundary layer flows. *J. Atmos. Sci.* **51**: 999–1022.
- Morrison H, Thompson G, Tatarskii V. 2009. Impact of cloud microphysics on the development of trailing stratiform precipitation in a simulated squall line: comparison of one- and two-moment schemes. *Mon. Weather Rev.* **137**: 991–1007.
- Nicholls ME, Pielke RA, Cotton WR. 1991. A two-dimensional numerical investigation of the interaction between sea breezes and deep convection over the Florida peninsula. *Mon. Weather Rev.* **119**: 298–323.
- Niyogi D, Holt T, Zhong S, Pyle PC, Basara J. 2006. Urban and land surface effects on the 30 July 2003 mesoscale convective system event observed in the southern Great Plains. *J. Geophys. Res.* **111**: D19107. <https://doi.org/10.1029/2005JD006746>.
- Ntelekos AA, Smith JA, Krajewski WF. 2007. Climatological analyses of thunderstorms and flash floods in the Baltimore metropolitan region. *J. Hydrol.* **8**: 88–101.
- Purdum JFW. 1976. Some uses of high resolution GOES imagery in the mesoscale forecasting of convection and its behavior. *Mon. Weather Rev.* **104**: 1474–1483.
- Rasmussen KL, Houze RA Jr. 2011. Orographic convection in subtropical South America as seen by the TRMM satellite. *Mon. Weather Rev.* **139**: 2399–2420.
- Rasmussen KL, Houze RA Jr. 2016. Convective initiation near the Andes in subtropical South America. *Mon. Weather Rev.* **144**: 2351–2374.
- Rhea JO. 1966. A study of thunderstorm formation along drylines. *J. Appl. Meteorol.* **5**: 58–63.
- Romanschke U, Medina S, Houze RA Jr. 2010. Regional, seasonal, and diurnal variations of extreme convection in the South Asian region. *J. Clim.* **23**: 419–439.
- Rozoff CM, Cotton WR, Adegoke JO. 2003. Simulation of St. Louis, Missouri, land use impacts on thunderstorms. *J. Appl. Meteorol.* **42**: 716–738.
- Schneiderer M, Schär C. 2000. Idealised numerical experiments of Alpine flow regimes and southside precipitation events. *Meteorol. Atmos. Phys.* **72**: 233–250.
- Shem W, Shepherd M. 2009. On the impact of urbanization on summertime thunderstorms in Atlanta: Two numerical model case studies. *Atmos. Res.* **92**: 172–189.
- Sheng C, Gao S, Shi Y. 2012. Numerical simulation of the dynamic effect of the orography on a Mentougou severe torrential rain event. *Acta Meteorol. Sin.* **70**: 65–77 (in Chinese with English Abstract).
- Shepherd JM, Carter M, Manyin M, Messen D, Burian S. 2010. The impact of urbanization on current and future coastal precipitation: A case study for Houston. *Environ. Plann. B: Plann. Des.* **37**: 284–304.
- Stauffer DR, Seaman NL. 1990. Use of four-dimensional data assimilation in a limited-area mesoscale model. Part I: Experiments with synoptic-scale data. *Mon. Weather Rev.* **118**: 1250–1277.
- Stauffer DR, Seaman NL. 1994. Multiscale four-dimensional data assimilation. *J. Appl. Meteorol.* **33**: 416–434.
- Stauffer DR, Seaman NL, Binkowski FS. 1991. Use of four-dimensional data assimilation in a limited-area mesoscale model. Part II: Effects of data assimilation within the planetary boundary layer. *Mon. Weather Rev.* **119**: 734–754.
- Sun J, Yang B. 2008. Meso- β scale torrential rain affected by topography and the urban circulation. *Chin. J. Atmos. Sci.* **32**: 1352–1364 (in Chinese with English Abstract).
- Sun J, Wang H, Wang L, Liang F, Kang Y, Jiang X. 2006. The role of urban boundary layer in local convective torrential rain happening in Beijing on 10 July 2004. *Chin. J. Atmos. Sci.* **30**: 221–234 (in Chinese with English Abstract).
- Thielen J, Wobrock W, Gadian A, Mestayer PG, Creutin JD. 2000. The possible influence of urban surfaces on rainfall development: a sensitivity study in 2D in the meso- γ -scale. *Atmos. Res.* **54**: 15–39.
- Tripoli GJ, Cotton WR. 1989a. Numerical study of an observed orogenic mesoscale convective system. Part I: Simulated genesis and comparison with observations. *Mon. Weather Rev.* **117**: 273–304.
- Tripoli GJ, Cotton WR. 1989b. Numerical study of an observed orogenic mesoscale convective system. Part II: Analysis of governing dynamics. *Mon. Weather Rev.* **117**: 305–328.
- Tucker DF, Crook NA. 1999. The generation of a mesoscale convective system from mountain convection. *Mon. Weather Rev.* **127**: 1259–1273.
- Wang H, Sun JS. 2008. Effects of underlying surface physical process on a severe hail event occurred in Beijing area. *Meteorol. Mon.* **34**: 16–21 (in Chinese with English Abstract).
- Wang CC, Chen GTJ, Chen TC, Tsuboki K. 2005. A numerical study on the effects of Taiwan topography on a convective line during the Mei-Yu season. *Mon. Weather Rev.* **133**: 3217–3242.
- Weckwerth TM, Parsons DB. 2006. A review of convective initiation and motivation for IHOP_2002. *Mon. Weather Rev.* **134**: 5–22.
- Weckwerth TM, Wakimoto RM. 1992. The initiation and organization of convective cells atop a cloud-air outflow boundary. *Mon. Weather Rev.* **120**: 2169–2187.
- Weckwerth TM, Bennett LJ, Miller LJ, van Baelen J, di Girolamo P, Blyth AM, Hertnecky TJ. 2014. An observational and modeling study of the processes leading to deep, moist convection in complex terrain. *Mon. Weather Rev.* **142**: 2687–2708.
- Whiteman CD. 2000. *Mountain Meteorology*. Oxford University Press: Oxford.
- Wilhelmson RB, Chen CS. 1982. A simulation of the development of successive cells along a cold outflow boundary. *J. Atmos. Sci.* **39**: 1466–1483.
- Wilson JW, Mueller CK. 1993. Nowcasts of thunderstorm initiation and evolution. *Weather and Forecasting* **8**: 113–131.
- Wilson JW, Robert RD. 2006. Summary of convective storm initiation and evolution during IHOP: Observational and modeling perspective. *Mon. Weather Rev.* **134**: 23–47.
- Wilson JW, Schreiber WE. 1986. Initiation of convective storms at radar-observed boundary-layer convergence lines. *Mon. Weather Rev.* **114**: 2516–2536.
- Wulfmeyer V, Behrendt A, Bauer H-S, Kottmeier C, Corsmeier U, Blyth A, Craig G, Schumann U, Hagen M, Crewell S, Di Girolamo P, Flamant C, Miller M, Montani A, Mobbs SD, Richard E, Rotach MW, Arpagaus M, Russchenberg H, Schlüssel P, König M, Gärtner V, Steinacker R, Dorninger M, Turner DD, Weckwerth T, Hense A, Simmer C. 2008. The Convective and Orographically induced Precipitation Study. *Bull. Am. Meteorol. Soc.* **89**: 1477–1486.
- Xu L, Raman S, Madala RV, Hodur R. 1996. A non-hydrostatic modeling study of surface moisture effects on mesoscale convection induced by sea breeze circulation. *Meteorol. Atmos. Phys.* **58**: 103–122.
- Xue M, Martin WJ. 2006. A high-resolution modeling study of the 24 May 2002 dryline case during IHOP. Part I: Numerical simulation and general evolution of the dryline and convection. *Mon. Weather Rev.* **134**: 149–171.
- Young GS, Kristovich DAR, Hjelmfelt MR, Foster RC. 2002. Rolls, streets, waves, and more: A review of quasi-two-dimensional structures in the atmospheric boundary layer. *Bull. Am. Meteorol. Soc.* **83**: 997–1001.
- Zhang DL, Fritsch JM. 1986. Numerical simulation of the meso-beta-scale structure and evolution of the 1977 Johnstown flood. Part I: Model description and verification. *J. Atmos. Sci.* **43**: 1913–1943.
- Zhang DL, Fritsch JM. 1988. Numerical simulation of the meso-beta-scale structure and evolution of the 1977 Johnstown flood. Part III: Internal gravity waves and the squall line. *J. Atmos. Sci.* **45**: 1252–1268.
- Zhang DL, Shou YX, Dickerson RR. 2009. Upstream urbanization exacerbates urban heat island effects. *Geophys. Res. Lett.* **36**: L24401. <https://doi.org/10.1029/2009GL041082>.
- Zhang DL, Shou YX, Dickerson RR, Chen F. 2011. Impact of upstream urbanization on the urban heat island effects over the Washington–Baltimore metropolitan region. *J. Appl. Meteorol. Climatol.* **50**: 2012–2029.
- Zhang DL, Lin Y, Zhao P, Yu X, Wang S, Kang H, Ding Y. 2013. The Beijing extreme rainfall of 21 July 2012: ‘right results’ but for wrong reasons. *Geophys. Res. Lett.* **40**: 1426–1431. <https://doi.org/10.1002/grl.50304>.
- Zhong L, Mu R, Zhang DL, Zhao P, Zhang Z, Wang N. 2015. An observational analysis of warm-sector rainfall characteristics associated with the 21 July 2012 Beijing extreme rainfall event. *J. Geophys. Res. Atmos.* **120**: 3274–3291. <https://doi.org/10.1002/2014JD022686>.
- Ziegler CL, Lee TJ, Pielke RA. 1997. Convective initiation at the dryline: A modeling study. *Mon. Weather Rev.* **125**: 1001–1026.